J|A|C|S
ARTICLES
Published on Web 09/13/2005

Insight into Enzymatic C−F Bond Formation from QM and QM/MM Calculations

Hans Martin Senn,*,† David O'Hagan,‡ and Walter Thiel*,†

Contribution from the Max-Planck-Institut für Kohlenforschung, D-45470 Mülheim an der Ruhr, Germany, and the School of Chemistry and Centre for Biomolecular Science, University of St. Andrews, St. Andrews, KY16 9ST, U.K.

Received June 13, 2005; E-mail: senn@mpi-muelheim.mpg.de; thiel@mpi-muelheim.mpg.de

Downloaded via UNIV ILLINOIS URBANA-CHAMPAIGN on June 1, 2022 at 22:01:53 (UTC).
See https://pubs.acs.org/sharingguidelines for options on how to legitimately share published articles.

Abstract: The C−F bond-forming step in the fluorinase, the only native fluorination enzyme characterized to date, has been studied. The enzyme catalyzes the reaction between *S*-adenosyl-L-methionine (SAM) and fluoride ions to form 5′-fluoro-5′-deoxyadenosine (5′-FDA) and L-methionine. To obtain an insight into the mechanism of this unusual enzymatic reaction and to elucidate the role of the enzyme in catalysis, we have explored the conformational energetics of SAM and the intrinsic reactivity patterns of SAM and fluoride with DFT (BP86) and continuum solvent methods, before investigating the full enzymatic system with combined DFT/CHARMM calculations. We find that the enzymatic reaction follows an S_N2 reaction mechanism, concurring with the intrinsic reactivity preferences in solution. The formation of sulfur ylides is thermodynamically strongly disfavored, and an alternative elimination−addition mechanism involving the concerted anti-Markovnikov addition of HF to an enol ether is energetically viable, but kinetically prohibitive. The S_N2 activation energy is 92 (112) kJ mol^{-1} in solution, but only 53 (63) kJ mol^{-1} in the enzyme, and the reaction energy in the enzyme is −25 (−34) kJ mol^{-1} (values in parentheses are B3LYP single-point energies). The fluorinase thus lowers the barrier for C−F bond formation by 39 (49) kJ mol^{-1}. A decomposition analysis shows that the major role of the enzyme is in the preparation and positioning of the substrates.

1. Introduction

Fluorine substitution in organic compounds continues to enjoy an increasing profile due to the unique chemical properties which can result as a consequence of fluorine incorporation.[1−5] The ability to improve pharmacokinetics by fluorine substitution into bioactives secured their utility in the pharmaceuticals and agrochemicals sectors, and selectively fluorinated entities emerge as valuable products in the materials and the fine chemicals industries. Although fluorine is the most abundant halogen in the earth's crust,[6] its bioavailability is extremely low due to its propensity to form sparingly soluble salts with many inorganic cations. Moreover, the strongly negative hydration free energy of fluoride further impedes its uptake into the cell from aqueous media. Only about a dozen fluorine-containing natural products have been found so far,[7] and their biosynthesis has remained elusive until very recently. This contrasts with the other halometabolites, of which several thousands are known and whose enzymatic synthesis has been investigated in some detail.[8] Several halogenating enzymes, forming C−X bonds (X = Cl, Br, I) via different mechanisms, have been identified. Notably, iron- or vanadium-dependent haloperoxidases, flavin-($FADH_2$-)dependent halogenases,[9a] nonheme-iron halogenases depending on α-ketoglutarate and molecular oxygen,[9b−d] and methyltransferases that use *S*-adenosylmethionine (SAM) to produce halomethanes.[9e]

The first report of enzymatic C−F bond formation involved mutant glycosidases[10−13] that lack the nucleophilic carboxylate residue in the active site, a residue which stabilizes the intermediate oxocarbenium ion prior to disaccharide formation. Fluoride at high concentrations (2 M) is able to quench the oxocarbenium ion in these mutants and generate transient α-fluoromonosaccharides, which can act as surrogate electrophiles for disaccharide formation, and thus fluoride ion restores catalytic activity.

† Max-Planck-Institut für Kohlenforschung.
‡ University of St. Andrews.

(1) Hiyama, T. *Organofluorine Compounds: Chemistry and Application*; Springer: Berlin, 2000.
(2) *J. Fluorine Chem.* **2001**, *109*, 1−94.
(3) *ChemBioChem* **2004**, *5*, 557−726.
(4) Chambers, R. D. *Fluorine in Organic Chemistry*; Blackwell: Oxford, 2004.
(5) Kirsch, P. *Modern Fluoroorganic Chemistry: Synthesis, Reactivity, Applications*; Wiley-VCH: Weinheim, 2004.
(6) Emsley, J. *The Elements*, 2nd ed.; Clarendon Press: Oxford, 1991.
(7) Deng, H.; O'Hagan, D.; Schaffrath, C. *Nat. Prod. Rep.* **2004**, *21*, 773−784.
(8) Murphy, C. D. *J. Appl. Microbiol.* **2003**, *94*, 539−548.
(9) (a) Yeh, E.; Garneau, S.; Walsh, C. T. *Proc. Natl. Sci. U.S.A.* **2005**, *102*, 3960−3965. (b) Vaillancourt, F. H.; Yin, J.; Walsh, C. T. *Proc. Natl. Sci. U.S.A.* **2005**, *102*, 10111−10116. (c) Vaillancourt, F. H.; Yeh, E.; Vosburg, D. A.; O'Connor, S. E.; Walsh, C. T. *Nature* **2005**, *436*, 1191−1194. (d) Schnarr, N. A.; Khosla, C. *Nature* **2005**, *436*, 1094−1095. (e) Wuosmaa, A. M.; Hager, L. P. *Science* **1990**, *249*, 160−162.
(10) Nashiru, O.; Zechel, D. L.; Stoll, D.; Mohammadzadeh, T.; Warren, R. A. J.; Withers, S. G. *Angew. Chem., Int. Ed.* **2001**, *40*, 417−419.
(11) Zechel, D. L.; Reid, S. P.; Nashiru, O.; Mayer, C.; Stoll, D.; Jakeman, D. L.; Warren, R. A. J.; Withers, S. G. *J. Am. Chem. Soc.* **2001**, *123*, 4350−4351.
(12) Zechel, D. L.; Withers, S. G. *Curr. Opin. Chem. Biol.* **2001**, *5*, 643−649.
(13) Zechel, D. L.; Reid, S. P.; Stoll, D.; Nashiru, O.; Warren, R. A. J.; Withers, S. G. *Biochemistry* **2003**, *42*, 7195−7204.

Scheme 1. Conversion of SAM and F^- to 5′-FDA and L-methionine by the Fluorinase and Subsequent Downstream Metabolism of 5′-FDA to the Fluorometabolites Fluoroacetate and 4-Fluorothreonine

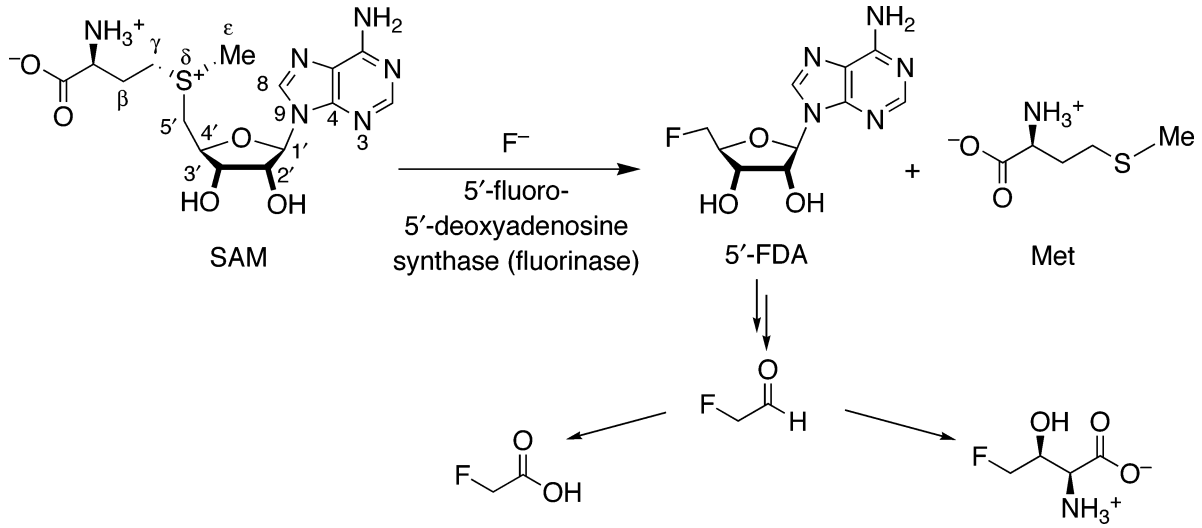

In 2002, the laboratory of one of us (D.O'H.) succeeded in identifying the first native fluorination enzyme.[14] Isolated from the bacterium *Streptomyces cattleya*, the enzyme catalyzes the reaction between SAM and fluoride ions to form 5′-fluoro-5′-deoxyadenosine (5′-FDA) and L-methionine. The product 5′-FDA is ultimately metabolized via fluoroacetaldehyde to the secondary metabolites fluoroacetate and 4-fluorothreonine (Scheme 1).[7,15] Subsequent cloning and overexpression of the enzyme has allowed crystals to be obtained that were suitable for X-ray diffraction analyses.[16]

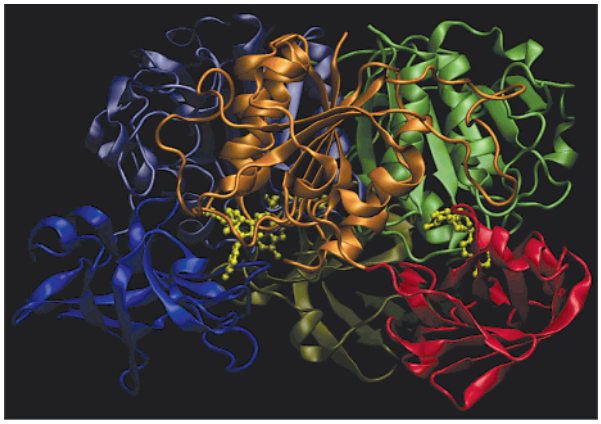

Figure 1. Representation of the SAM-bound trimeric structure of the fluorinase (PDB 1RQP). The N- and C-terminal domains of each chain are color-coded. Chain A, orange/red; chain B, ice-blue/blue; chain C, lime/tan. SAM is yellow.

The structural study revealed the following key findings.[17] The fluorinase (5′-FDA synthase, EC 2.5.1.63) is assembled from three 299-residue protein chains. The monomers are arranged around a 3-fold axis, contacting each other with their N-terminal domains, and then these trimers dimerize to form a hexamer. Despite purification, the structure contains three molecules of SAM per trimer (PDB accession code 1RQP, Figure 1). SAM is bound at the interface between the C-terminal domain of one chain and the N-terminal domain of the neighboring chain (Figure 2). Each of the components of SAM (adenine ring, ribose, L-methionine) is recognized by both monomers, suggesting a role in holding the chains together. Since SAM is completely buried inside the protein, the observed quaternary structure of the enzyme may gape during the catalytic cycle for the substrates SAM and fluoride to be bound and the products to be released. In the SAM-bound structure, no channels suitable for transporting fluoride to the active site are obvious, implying that fluoride may be bound first, followed by SAM, which then triggers the formation of the closed structure.

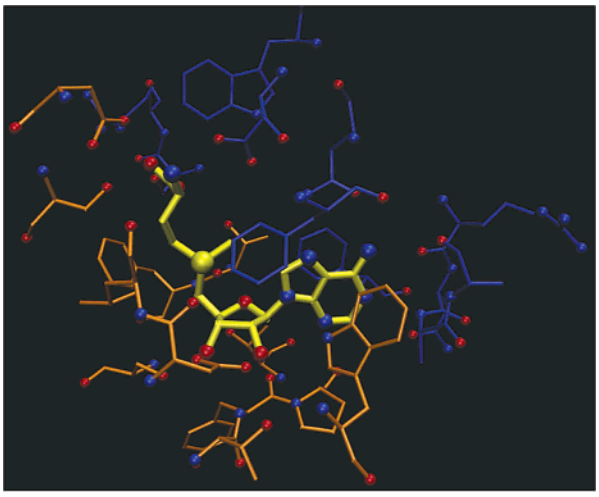

Figure 2. Active site with bound SAM (yellow). Residues from the N-terminal domain of chain A in orange; residues from the C-terminal domain of chain B in blue. Heteroatoms are shown as balls (O, red; N, blue; S, yellow).

A second X-ray structure was obtained in which the products, 5′-FDA and L-methionine, are still bound in the active site (PDB accession code 1RQR, Figure 3). The comparison to the SAM-bound complex reveals only minimal changes, except for slight shifts associated with the formation of the C5′−F bond and the cleavage of the C5′−S bond. The fluorine atom of the 5′-FDA

(14) O'Hagan, D.; Schaffrath, C.; Cobb, S. L.; Hamilton, J. T. G.; Murphy, C. D. *Nature* **2002**, *416*, 279−279.
(15) Schaffrath, C.; Cobb, S. L.; O'Hagan, D. *Angew. Chem., Int. Ed.* **2002**, *41*, 3913−3915.
(16) Dong, C.; Deng, H.; Dorward, M.; Schaffrath, C.; O'Hagan, D.; Naismith, J. H. *Acta Crystallogr., Sect. D* **2003**, *59*, 2292−2293.
(17) Dong, C.; Huang, F.; Deng, H.; Schaffrath, C.; Spencer, J. B.; O'Hagan, D.; Naismith, J. H. *Nature* **2004**, *427*, 561−565.

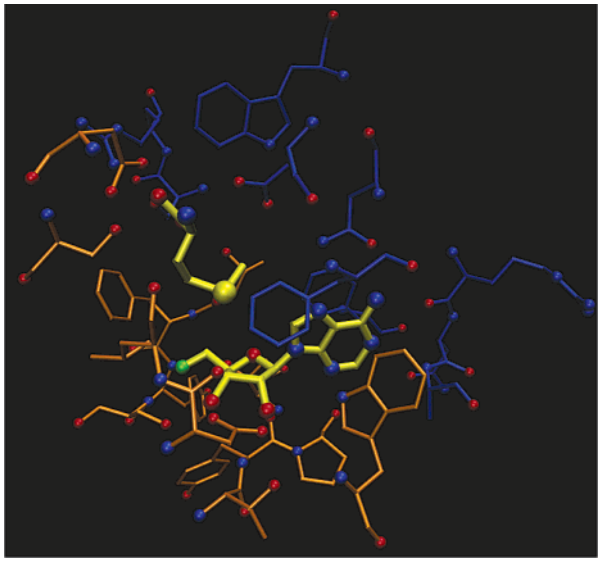

Figure 3. Active site with bound products 5′-FDA and L-methionine (both yellow). Coloring as that in Figure 2.

fluoromethyl group occupies a hydrophobic pocket that was empty in the SAM-bound structure and accepts hydrogen bonds from residues lining the pocket. The size of the pocket (1.4−1.6 Å) may account for the preference of the enzyme for fluoride over the other halides. Other conceivable factors include the specific hydrogen-bonding pattern and the electrostatic environment. There are no water molecules in the vicinity, suggesting that fluoride must be fully dehydrated in the active site. The position and conformation of SAM in the reactant complex as compared to the bound products after the reaction is indicative of an S_N2 mechanism. This notion is supported by stereochemical studies involving isotope labeling that have established that the C−S bond is cleaved and the C−F bond formed by a process involving an inversion of configuration at C5′.[18,19]

Another notable point is that SAM acts here as a nucleoside (5′-deoxyadenosyl) donor. In the majority of biological reactions involving SAM,[20] the cofactor serves as a methylating agent,[21,22] as illustrated by the halomethane-producing methyltransferases.[9] In a few cases, SAM transfers the 2-aminobutanoate moiety.[20] Only the "radical SAM" enzymes, which have been the subject of active research in recent years,[23,24] cleave the C5′−S bond of SAM after one-electron reduction to generate L-methionine and a 5′-deoxyadenosyl radical, which then abstracts hydrogen from a substrate. This homolytic reaction pathway is, however, quite different from the heterolytic group-transfer chemistry otherwise associated with SAM enzymes. The fluorinase therefore appears to be the first case where the 5′-carbon of the adenosyl moiety of SAM is attacked by a nucleophile.

In the present contribution, we have investigated the C−F bond-forming step catalyzed by the fluorinase by means of density-functional theory (DFT) and combined quantum-mechanical/molecular-mechanical (QM/MM) calculations. The conformational preferences of SAM have been evaluated, and DFT with a continuum solvent model has been used to explore the intrinsic reactivity of SAM toward fluoride and the energetics of different reaction channels. The full enzymatic system was then examined using QM/MM methods by determining minima and transition states for C−F bond formation. A combining of the results from both studies has allowed us to elucidate the role of the enzyme in this reaction and in particular to reveal how it activates the substrates through both conformational and orientational preorganization, hydrogen bonding, and specific environmental effects within the binding pocket.

II. Computational Methods

A. DFT Calculations. The program package TURBOMOLE[25−29] was used for all DFT calculations. The resolution of the identity (RI) approximation[30−33] was employed with the gradient-corrected functionals for exchange and correlation due to Becke[34] and Perdew,[35−37] respectively (BP86). Single-point energy calculations on BP86-optimized structures were performed in selected cases using the B3LYP hybrid functional[34,35,38−41] as implemented in TURBOMOLE. We used the standard TURBOMOLE TZVP basis[42] (valence triple-ζ with one polarization function on all atoms), augmented by diffuse functions on all atoms to give a basis set we refer to as TZVP+. Electrostatic solvation effects were described within the conductor-like screening model[43,44] (COSMO) as implemented in TURBOMOLE.[45] The relative permittivity was $\epsilon_r = 78.4$, corresponding to H_2O at 298 K. The solvation radii were reparametrized to reproduce the experimental solvation free energies for a set of reference compounds akin to the molecules investigated. Geometries were optimized in redundant internal coordinates[46] and stationary points characterized by calculating vibrational frequencies analytically[29,47,48] (in the gas phase) or by finite differences (with continuum solvent). For transition-state (TS) searches, TURBOMOLE provided energy and gradient for a linear-scaling microiterative algorithm working in hybrid delocalized coordinates[49] (HDLCOpt) implemented in ChemShell.[50,51] In this scheme, the system

(18) O'Hagan, D.; Goss, R. J. M.; Meddour, A.; Courtieu, J. *J. Am. Chem. Soc.* **2003**, *125*, 379−387.
(19) Cadicamo, C. D.; Courtieu, J.; Deng, H.; Meddour, A.; O'Hagan, D. *ChemBioChem* **2004**, *5*, 685−690.
(20) Fontecave, M.; Atta, M.; Mulliez, E. *Trends Biochem. Sci.* **2004**, *29*, 243−249.
(21) Chiang, P. K.; Gordon, R. K.; Tal, J.; Zeng, G. C.; Doctor, B. P.; Pardhasaradhi, K.; McCann, P. P. *FASEB J.* **1996**, *10*, 471−480.
(22) Schubert, H. L.; Blumenthal, R. M.; Cheng, X. *Trends Biochem. Sci.* **2003**, *28*, 329−335.
(23) Frey, P. A.; Magnusson, O. T. *Chem. Rev.* **2003**, *102*, 2129−2148.
(24) Layer, G.; Heinz, D. W.; Jahn, D.; Schubert, W.-D. *Curr. Opin. Chem. Biol.* **2004**, *8*, 468−476.
(25) *TURBOMOLE*, V. 5.7.1, 2004.
(26) Ahlrichs, R.; Bär, M.; Häser, M.; Horn, H.; Kölmel, C. *Chem. Phys. Lett.* **1989**, *162*, 165−169.
(27) Treutler, O.; Ahlrichs, R. *J. Chem. Phys.* **1995**, *102*, 346−354.
(28) Häser, M.; Ahlrichs, R. *J. Comput. Chem.* **1989**, *10*, 104−111.
(29) Horn, H.; Weiss, H.; Häser, M.; Ehrig, M.; Ahlrichs, R. *J. Comput. Chem.* **1991**, *12*, 1058−1064.
(30) Eichkorn, K.; Treutler, O.; Öhm, H.; Häser, M.; Ahlrichs, R. *Chem. Phys. Lett.* **1995**, *240*, 283−289.
(31) Eichkorn, K.; Treutler, O.; Öhm, H.; Häser, M.; Ahlrichs, R. *Chem. Phys. Lett.* **1995**, *242*, 652−660.
(32) Eichkorn, K.; Weigend, F.; Treutler, O.; Ahlrichs, R. *Theor. Chem. Acc.* **1997**, *97*, 119−124.
(33) von Arnim, M.; Ahlrichs, R. *J. Comput. Chem.* **1998**, *19*, 1746−1757.
(34) Becke, A. D. *Phys. Rev. A* **1988**, *38*, 3098−3100.
(35) Vosko, S. H.; Wilk, L.; Nusair, M. *Can. J. Phys.* **1980**, *58*, 1200−1211.
(36) Perdew, J. P. *Phys. Rev. B* **1986**, *33*, 8822−8824.
(37) Perdew, J. P. *Phys. Rev. B* **1986**, *34*, 7406.
(38) Stephens, P. J.; Devlin, J. F.; Chabalowski, C. F.; Frisch, M. J. *J. Phys. Chem.* **1994**, *98*, 11623−11627.
(39) Becke, A. D. *J. Chem. Phys.* **1993**, *98*, 5648−5652.
(40) Lee, C.; Yang, W.; Parr, R. G. *Phys. Rev. B* **1988**, *37*, 785−789.
(41) Hertwig, R. H.; Koch, W. *Chem. Phys. Lett.* **1997**, *268*, 345−351.
(42) Schäfer, A.; Huber, C.; Ahlrichs, R. *J. Chem. Phys.* **1994**, *100*, 5829−5835.
(43) Klamt, A. In *Encyclopedia of Computational Chemistry*; Schleyer, P. v. R., Ed.; Wiley: Chichester, 1998; Vol. 1, pp 604−615.
(44) Klamt, A.; Schüürmann, G. *J. Chem. Soc., Perkin Trans. 2* **1993**, 799−805.
(45) Schäfer, A.; Klamt, A.; Sattel, D.; Lohrenz, J. C. W.; Eckert, F. *Phys. Chem. Chem. Phys.* **2000**, *2*, 2187−2193.
(46) von Arnim, M.; Ahlrichs, R. *J. Chem. Phys.* **1999**, *111*, 9183−9190.
(47) Deglmann, P.; Furche, F.; Ahlrichs, R. *Chem. Phys. Lett.* **2002**, *362*, 511−518.
(48) Deglmann, P.; Furche, F. *J. Chem. Phys.* **2002**, *117*, 9535−9538.
(49) Billeter, S. R.; Turner, A. J.; Thiel, W. *Phys. Chem. Chem. Phys.* **2000**, *2*, 2177−2186.

is partitioned into a core region, for which the Hessean is calculated, and a number of residues. Further details on basis set, solvation radii, and HDLC residue partitioning are provided as Supporting Information.

B. System Preparation, Classical Simulations. The structure of the SAM−enzyme complex obtained from the Protein Data Bank (PDB 1RQP) contains the trimeric unit, with the first seven and the last residues of each chain missing, and 719 water molecules. The program Reduce[52,53] was used to add hydrogen atoms and adjust the orientation of Asn, Gln, and His side chains, taking into account H-bonding networks as well as steric considerations. The orientation and protonation state of all His residues were re-evaluated manually. Hydration and preparatory classical minimization and molecular dynamics (MD) runs were performed with the program CHARMM[54−56] with the combined all-hydrogen force fields CHARMM22[57] (proteins) and CHARMM27[58,59] (nucleic acids). We developed the parameters for SAM based on those for *S*-adenosylhomocysteine, obtained from MacKerell.[60] The F^- parameters were provided by Roux.[61,62] We defined an active region including all residues within 15 Å of the S atom of SAM in chain A, SAM(A):S. All other atoms were kept fixed. A 25-Å sphere of equilibrated water molecules was centered on SAM(A):S, and those water molecules too close to existing atoms were deleted. All water molecules (i.e., crystallographic and added) in the 25-Å sphere were geometry-optimized and subjected to an MD run of 100 ps at 300 K. The water molecules were kept internally rigid and subject to spherical boundary conditions. We performed six such hydration cycles until the number of added water molecules was approximately constant. The residues within the 15-Å sphere, initially kept fixed, were gradually released using positional restraints. An MD simulation of 1 ns without restraints concluded the preparation of the SAM−enzyme complex. By comparing the structure of SAM and its surroundings over the MD simulation to the X-ray structure, we validated the SAM parametrization. Since no experimental structure with bound F^- is available, we manually placed the fluoride ion at about equal distances to potential H-bond donors into the empty pocket identified in the structure of the SAM−enzyme complex. Using the same definitions for the active region as above, the initial structure for this reactant complex was geometry-optimized, subjected to about 300 ps of unrestrained MD, rehydrated, and finally run for 1 ns. See the Supporting Information for full details on the CHARMM parameter development and the hydration procedure.

C. QM/MM Setup. All QM/MM calculations were carried out at the DFT(BP86)/CHARMM level with the modular program package ChemShell.[50,51] QM energy and gradient were provided by TURBOMOLE, interfaced to ChemShell. MM energy and gradient were evaluated by ChemShell's internal force-field driver using the CHARMM topology and parameter data; the MM electrostatic interactions were fully calculated. The QM electron density was electrostatically embedded into the field of the rigid MM point charges by including them into the QM Hamiltonian. The charge-shift scheme was applied at the QM/MM boundary;[51] no electrostatic QM/MM cutoff was employed. The QM part contained SAM without the 2-ammoniopropanoate moiety, that is, 5′-(*S*,*S*-dimethylsulfonio)-5′-deoxyadenosine, the covalent bond across the QM/MM boundary being saturated with a H link atom. For the reactant complex, F^- was also part of the QM region, which thus included 38 (39 with F^-) atoms. This partitioning coincides with the CHARMM charge-group boundaries, providing an MM region with integer charge and a neutral QM region in case of the reactant complex. The bond across the QM/MM boundary is an "innocent" C−C single bond. QM/MM geometry optimizations were performed with a linear-scaling microiterative algorithm working in hybrid delocalized coordinates.[49] All residues and water molecules within 8 Å of SAM, or of SAM or F^-, respectively, were included in the optimization; the remaining atoms were kept fixed. The residues for the optimization algorithm were chosen as the standard amino acid residues. In transition-state searches, the core region, for which the Hessean is calculated, included F^-, C5′H$_2$, and Sδ. The setup of the two QM/MM systems (SAM−enzyme complex and reactant complex including F^-) is summarized in Table 1. Refer to the Supporting Information for additional details on the active region and the HDLC residue partitioning.

Table 1. Setup of QM/MM Systems

no. of atoms	SAM−enzyme complex		reactant complex	
total (water)	17 556	(4233)	17 596	(4272)
active region (water)	1333	(99)	1394	(111)
QM part	38		39	

III. Results and Discussion

A. QM Calculations. 1. Conformational Survey. (a) Enzyme-Bound SAM. The structure of SAM in the SAM-fluorinase complex possesses remarkable conformational features. The furanose ring adopts an almost ideal envelope conformation, with O4′ as the "tip" of the envelope, that is, furanose-^{O}E or O4′-endo (the exo/endo descriptor designates the orientation relative to the C4′ substituent.) The average phase angle of pseudorotation is $P = 88°$; the average degree of pucker is $\psi_m = 43°$.[63−65] The endocyclic torsion angle about C2′−C3′, $\nu_2 \equiv \angle$(C1′, C2′, C3′, C4′), is only 1.6° (average from the three monomer chains). Moreover, the C2′- and C3′-hydroxy groups are oriented nearly perfectly synperiplanar, the average exocyclic torsion $\theta \equiv \angle$(O2′, C2′, C3′, O3′) being 2.8°. These conformational features are exceedingly rare. We therefore first investigate the factors determining the conformation of SAM and the energetics associated with conformational changes.

While not aiming at a comprehensive conformational study, we reconstruct SAM from simpler building blocks to analyze systematically the factors influencing the conformational preferences. Starting from tetrahydrofuran (THF), which provides the five-membered ring as the basic scaffold, we have added the C2′- and C3′-hydroxy groups, followed by the 1′-adenyl substituent, before examining SAM itself. We refer to the literature[66−71] for computational conformational studies of nucleotides, their building blocks, and models thereof.

(50) *ChemShell*, V. 3.0a3, 2004.
(51) Sherwood, P. et al. *THEOCHEM* **2003**, *632*, 1−28.
(52) Word, M. J. *Reduce*, V. 2.21; Biochemistry Department, Duke University: Durham, NC, 2003.
(53) Word, J. M.; Lovell, S. C.; Richardson, J. S.; Richardson, D. C. *J. Mol. Biol.* **1999**, *285*, 1735−1747.
(54) *CHARMM*, V. c31b1, 2004.
(55) Brooks, B. R.; Bruccoleri, R. E.; Olafson, B. D.; States, D. J.; Swaminathan, S.; Karplus, M. *J. Comput. Chem.* **1983**, *4*, 187−217.
(56) MacKerell, A. D., Jr.; Brooks, B.; Brooks, C. L., III; Nilsson, L.; Roux, B.; Won, Y.; Karplus, M. In *Encyclopedia of Computational Chemistry*; Schleyer, P. v. R., Ed.; Wiley: Chichester, 1998; Vol. 1, pp 271−277.
(57) MacKerell, A. D., Jr. et al. *J. Phys. Chem. B* **1998**, *102*, 3586−3616.
(58) Foloppe, N.; MacKerell, A. D., Jr. *J. Comput. Chem.* **2000**, *21*, 86−104.
(59) MacKerell, A. D., Jr.; Banavali, N. K. *J. Comput. Chem.* **2000**, *21*, 105−120.
(60) MacKerell, A. D., Jr. Personal communication, 2004.
(61) Roux, B. Personal communication, 2004.
(62) Miloshevsky, G. V.; Jordan, P. C. Personal communication, 2004.
(63) The pseudorotation in furanoses is characterized by two parameters: The phase angle $P = \text{atan}\{[\nu_4 + \nu_1 - \nu_3 - \nu_0]/[2\nu_2(\sin 36° + \sin 72°)]\}$ and the degree of pucker $\psi_m = \nu_2/\cos P$. Note that the endocyclic torsion angles ν_i were previously designated by τ_i and the degree of pucker by τ_m. If $\nu_2 < 0$, $P := P + 180°$.
(64) Altona, C.; Sundaralingam, M. *J. Am. Chem. Soc.* **1972**, *94*, 8205−8212.
(65) IUPAC-IUB Joint Commission on Biochemical Nomenclature. *Pure Appl. Chem.* **1983**, *55*, 1273−1280.
(66) Foloppe, N.; MacKerell, A. D., Jr. *J. Phys. Chem. B* **1998**, *102*, 6669−6678.
(67) Foloppe, N.; Nilsson, L.; MacKerell, A. D., Jr. *Biopolymers* **2001**, *61*, 61−76.
(68) Brameld, K. A.; Goddard, W. A., III. *J. Am. Chem. Soc.* **1999**, *121*, 985−993.
(69) Leulliot, N.; Ghomi, M.; Scalmani, G.; Berthier, G. *J. Phys. Chem. A* **1999**, *103*, 8716−8724.

(b) THF. According to experimental[72−75] (X-ray and neutron diffraction,[72] rotational spectroscopy[74,75]) and ab initio data,[76] THF has a C_2-symmetric minimum structure, that is, a ${}^2_3T$ or ${}^3_2T$ twist conformation with $P = 0°$ or 180°, respectively. However, the potential-energy surface along the pseudorotation path is extremely flat for THF, the barrier for interconversion between the two degenerate twist forms being <1 kJ mol^{-1}.[74−76] The transition structure is the C_s-symmetric ${}^{O}E$-envelope conformation. DFT methods have difficulties in reliably reproducing the correct energy ordering of the two symmetric conformations, and they often predict unsymmetric C_1 minimum structures. The results depend on the functional, the basis set, and the integration grid used.[76] We have verified that the energy difference $\Delta E = E(C_s) - E(C_2)$ is ±1 kJ mol^{-1} or smaller for several functionals (BP86, BLYP, PBE, B3LYP) with our standard setup (TZVP+ basis set, grid m3); the BP86 functional yields $\Delta E_{BP86} = -0.9$ kJ mol^{-1}. Using a very fine grid and very tight convergence criteria, we obtain $\Delta E_{BP86} = 0.04$ kJ mol^{-1}. However, neither the C_2 nor the C_s conformation are identified as minima but have one imaginary vibration. They both converge to the C_1-symmetric ${}^{O}T_4$ conformer **1** with $P = 73°$ and $\psi_m = 42°$, which lies −0.3 kJ mol^{-1} lower in energy at this level of theory. Reoptimizing with water as the continuum solvent does not change the structure appreciably. We conclude that conformational changes along the pseudorotation pathway are essentially unhindered in unsubstituted THF, consistent with experiment.[74,75]

(c) Dihydroxy-THF. We next investigate *cis*-2,3-dihydroxy-THF (**2**), considering two conformational degrees of freedom: (1) the direction of the hydroxy groups relative to the ring plane, either both pointing "down" or both pointing "up"; (2) the orientation of the O−H bonds, that is, rotations about C−O(H). There are three idealized rotamers about each C−O(H) bond that orient the O−H bonds gauche or anti with respect to C2−C3, which controls the possible intramolecular hydrogen bonds. Based on the optimized THF structure **1** with ${}^{O}T_4$ conformation, we created all 18 idealized structures for *cis*-2,3-dihydroxy-THF and used them as starting points for geometry optimizations. They afforded seven distinct minimum structures (not counting enantiomers), which can be classified according to the ring conformation (as expressed by the phase angle and the corresponding conformational descriptor) and the number and type of hydrogen bonds, as shown in Figure 4 and summarized in Table 2. The most stable conformer, **2.1**, features two hydrogen bonds, a strong one between the OH groups and a weaker one from O2−H to the ring oxygen O4. **2.2** and **2.3a**−**d** all have one hydrogen bond between the two OH groups; they are destabilized by 4 to 8 kJ mol^{-1} relative to **2.1**. Conformer **2.4**, where the O−H bonds are oriented such that the formation of a hydrogen bond is precluded, is 31 kJ mol^{-1} less stable than **2.1**. This provides an estimate for the H-bond stabilization energy of 20−30 kJ mol^{-1}. The OH groups are in all cases arranged synclinal to each other (or synperiplanar close to sc, respectively). With regard to ring conformation, only **2.1** is O4-exo; that is, O4 is on the same side as the OH groups, which makes the O2−H···O4 interaction possible. All other conformers are C4-exo, and **2.3a**−**d** and **2.4** are also all C3-endo, which thus makes C3-endo-C4-exo (i.e., ${}^3T_4$) the preferred conformation. Note, however, that the energetics is dominated by the presence or absence of hydrogen bonds, not by the ring conformation.

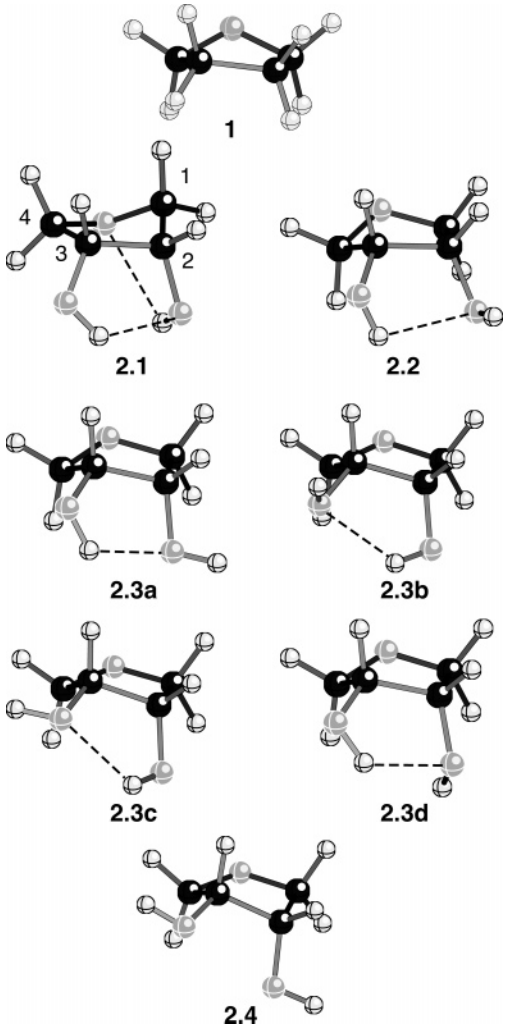

Figure 4. Conformers of THF (**1**) and *cis*-2,3-dihydroxy-THF (**2**).

Table 2. Conformers of *cis*-2,3-Dihydroxy-THF (**2**)

	ΔE/(kJ mol^{-1})[a]	P[b]	ring conformation[b]	H-bonds D···A	H-bonds d/Å	θ[c]
2.1	0	299°	${}^1T_O$	O3−H···O2	1.998	28°
				O2−H···O4	2.449	
2.2	3.9	66°	${}^OT_4$	O3−H···O2	2.228	26°
2.3a	5.9	46°	${}^3T_4$	O3−H···O2	2.042	35°
2.3b	6.7	43°	${}^3T_4$	O2−H···O3	2.044	31°
2.3c	8.0	36°	${}^3_4T$	O2−H···O3	2.103	40°
2.3d	6.7	49°	${}^3T_4$	O3−H···O2	2.048	30°
2.4	30.8	22°	${}^3T_4$			45°

[a] Electronic energy relative to **2.1**. [b] Pseudorotation phase angle and conformational descriptor according to refs 58, 64, and 65. The pucker amplitudes ψ_m are between 40° and 46°. [c] Exocyclic torsion about C2−C3, $\theta \equiv \angle$(O2, C2, C3, O3).

(d) Adenyl-Dihydroxy-THF. To generate different conformers of (1′*R*,2′*R*,3′*R*)-1′-adenyl-2′,3′-dihydroxy-THF (**3**), we

(70) Hocquet, A.; Leulliot, N.; Ghomi, M. *J. Phys. Chem. B* **2000**, *104*, 4560−4568.
(71) Markham, G. D.; Norrby, P.-O.; Bock, C. W. *Biochemistry* **2002**, *41*, 7636−7646.
(72) David, W. I. F.; Ibberson, R. M. *Acta Crystallogr., Sect. C* **1992**, *48*, 301−303.
(73) Cadioli, B.; Gallinella, E.; Coulombeau, C.; Jobic, H.; Berthier, G. *J. Phys. Chem.* **1993**, *97*, 7844−7856.
(74) Meyer, R.; López, J. C.; Alonso, J. L.; Melandri, S.; Favero, P. G.; Caminati, W. *J. Chem. Phys.* **1999**, *111*, 7871−7880.
(75) Melnik, D. G.; Gopalakrishnan, S.; Miller, T. A.; De Lucia, F. C. *J. Chem. Phys.* **2003**, *118*, 3589−3599.
(76) Strajbl, M.; Florián, J. *Theor. Chem. Acc.* **1998**, *99*, 166−170.

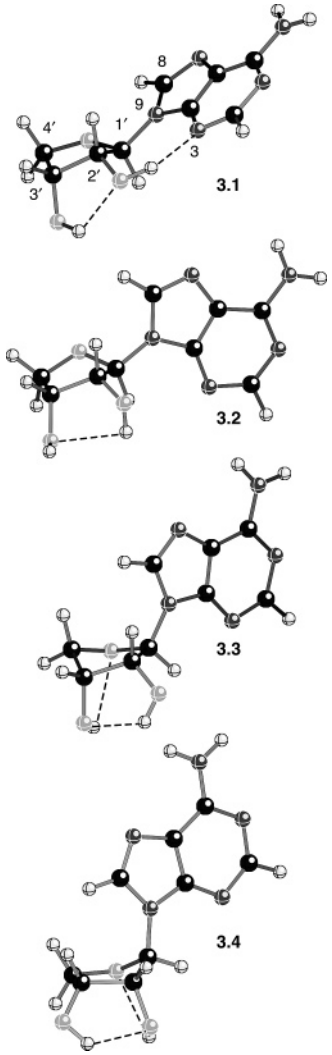

Figure 5. Conformers of (1′*R*,2′*R*,3′*R*)-1′-adenyl-2′,3′-dihydroxy-THF (**3**).

Table 3. Conformers of (1′*R*,2′*R*,3′*R*)-1′-Adenyl-2′,3′-dihydroxy-THF (**3**)

	Δ*E*/ (kJ mol^{-1})[a]	*P*[b]	ring conformation[b]	H-bonds D···A	*d*/Å	θ[c]	χ[d]
3.1	0	166°	$^{2}T_{3}$	O3′−H···O2′	2.097	−41°	169°
				O2′−H···N3	1.825		
3.2	30.1	122°	$^{O}T_{1}$	O2′−H···O3′	2.411	−31°	−124°
3.3	29.3	227°	$^{4}T_{3}$	O2′−H···O3′	2.061	−33°	−99°
				O3′−H···O4′	2.511		
3.4	35.2	304°	$^{1}T_{O}$	O3′−H···O2′	1.999	28°	−105°
				O2′−H···O4′	2.547		

[a] Electronic energy relative to **3.1**. [b] Pseudorotation phase angle and conformational descriptor according to refs 58, 64, and 65. The pucker amplitudes ψ_m are between 37° and 42°. [c] Exocyclic torsion about C2′−C3′, $\theta \equiv \angle$(O2′, C2′, C3′, O3′). [d] Exocyclic torsion about C1′−N9, $\chi \equiv \angle$(O4′, C1′, N9, C4).

started from **2.1** and **2.2** and their enantiomers, attaching the 1′-adenyl substituent trans to the OH groups in an idealized anti conformation about the C1′−N9 bond [$\chi \equiv \angle$(O4′, C1′, N9, C4) = −120°, that is, −anticlinal]. Geometry optimization provided the four conformers **3.1**−**4** (Figure 5, Table 3). Owing to its strong O2′−H···N3 hydrogen bond, **3.1** is the most stable conformer. However, the +antiperiplanar adenyl orientation renders it less relevant for our purposes as the orientation in the enzyme is −ac. Moreover, the strength of the hydrogen bond that stabilizes this orientation is overestimated in the gas phase relative to solution or the enzyme. The remaining conformers have the adenyl oriented −ac but differ in the ring pucker, which controls the direction (equatorial/axial) of the C1′−N9 bond. In **3.2**, the adenyl substituent is equatorial, while it is fully axial in **3.4**. In addition, **3.2** has only one relatively weak hydrogen bond between the OH groups, as compared to **3.3** and **3.4**. Still, it is at least as stable as the other −ac conformers, which suggests that it represents the preferred arrangement. The energetic penalty for axial adenyl is, however, small, **3.4** being only about 5 kJ mol^{-1} destabilized relative to **3.2**.

(e) SAM. Completing the reconstruction of SAM, we added the L-methionylmethyl substituent at C4′ of **3.1**−**4** in cis position with respect to adenyl. The initial conformation of the side chain was taken from the X-ray structure of the SAM−enzyme complex. Geometry optimization yielded the SAM conformers **4.1**−**3**, the structures generated from **3.3** and **3.4** having both converged to **4.3**. Another starting structure was obtained by taking the entire structure of SAM from the SAM−enzyme complex, affording **4.4**. The four conformers are shown in Figure 6; Table 4 lists relevant structural parameters and relative energies. The experimental structure of SAM from the SAM−enzyme complex is included for comparison. We use the neutral form of the amino acid (i.e., protonated carboxylic acid, unprotonated amino group) in gas-phase calculations.

As above, we disregard the conformer **4.1** because of its O2′−H···N3 hydrogen bond. **4.2** and **4.4** are conformationally very similar. They match in the ribose conformation, the orientation of the OH groups, the intramolecular H-bond, and the orientation of the adenyl. The only significant difference is the orientation of the methionyl chain [as expressed by the torsion $\phi \equiv \angle$(C5′, Sδ, Cγ, Cβ)], which leads to an energy difference of 4 kJ mol^{-1}. **4.3** differs from **4.2** mainly in the ribose conformation, which enables the formation of a stronger hydrogen bond between the OH groups, providing 15 kJ mol^{-1} of stabilization. Optimizing **4.3** in solution yields **4.3**(aq), where the ribose is now also in an O4′-endo conformation. (Note that for calculations in solvent, we use the zwitterionic form of the amino acid.) This $^{O}T_{4}$ conformation of the ring places both the 1′-adenyl and the 4′-methionylmethyl substituents equatorially, which is clearly sterically favorable.

A comparison with the X-ray structure of SAM(A) reveals that **4.2** is quite close, in particular with regard to ribose conformation and methionyl orientation. However, there is one major difference. In the X-ray structure of enzyme-bound SAM, the adenyl ring and the sulfonium methyl group nearly clash. The Cε−C8 distance is only 3.06 Å in SAM(A), significantly less than the sum of the van der Waals radii, which is 3.4 Å. In SAM(B) and SAM(C), this distance is 3.31 and 3.32 Å, respectively. In the conformers **4.1**−**4.4**, *d*(Cε, C8) is between 4.6 and 5.1 Å, well beyond the contact distance. The difference between the conformations of SAM(A) and **4.2** can be characterized by the following structural parameters. (i) Ring conformation: The ribose is almost ^{O}E in the experimental structures, which places the 1′-adenyl in a less equatorial arrangement than the $^{O}T_{1}$ conformation in **4.2** or **4.4**. This, in turn, pushes the adenyl toward the 4′-substituent. (ii) Adenyl orientation: In SAM(A, B, C), the adenyl ring is rotated about C1′−N9 such that C8−H points almost directly toward the sulfonium moiety. (iii) Sulfonium orientation: The torsion about C5′−Sδ, as measured by $\eta \equiv \angle$(C4′, C5′, Sδ, Cε), is only 63° in SAM(A),

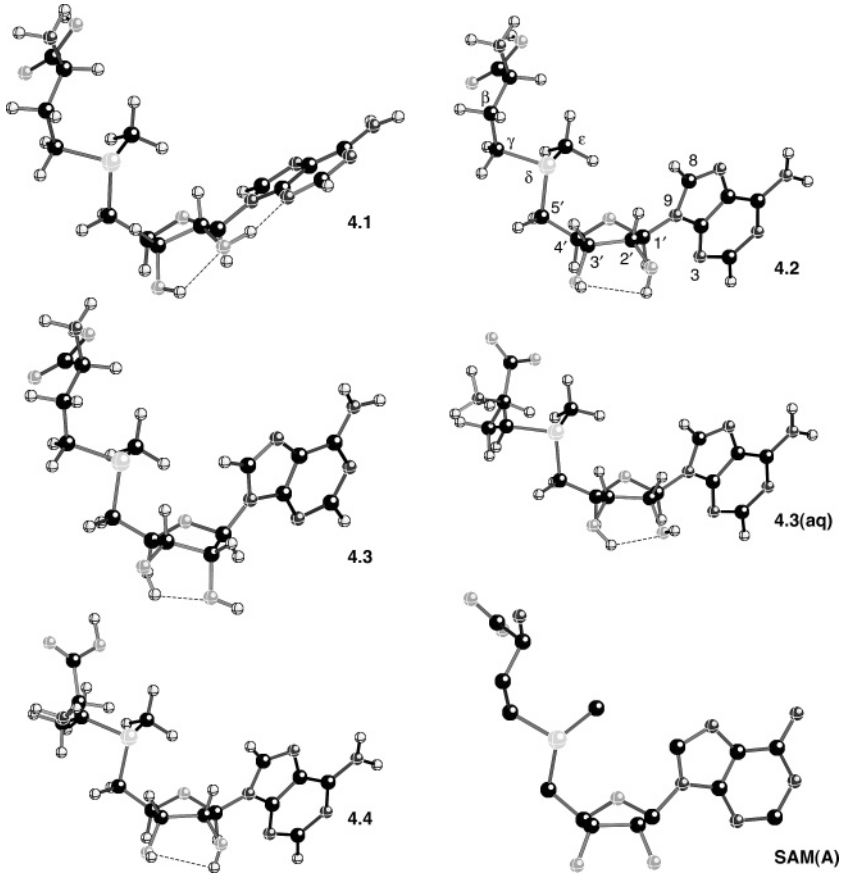

Figure 6. Conformers of SAM (**4**). SAM(A) is taken from PDB 1RQP.

Table 4. Conformers of SAM (**4**)

	ΔE/(kJ mol^{-1})[a]	P[b]	ring conformation[b]	H-bonds D···A	H-bonds d/Å	θ[c]	χ[d]	ϕ[e]
4.1	0	123°	$^{O}T_1$	O3′−H···O2′	2.041	−31°	150°	161°
				O2′−H···N3	1.760			
4.2	28.6	101°	$^{O}T_1$	O2′−H···O3′	2.516	−18°	−100°	159°
4.3	13.5	38°	$^{3}T_4$	O3′−H···O2′	2.096	39°	−104°	159°
4.4	24.8	100°	$^{O}T_1$	O2′−H···O3′	2.492	−18°	−98°	83°
4.3(aq)		80°	$^{O}T_4$	O3′−H···O2′	2.020	15°	−105°	100°
SAM(A)[f]		87°	$^{O}T_4$			−3°	−132°	149°

[a] Electronic energy relative to **4.1**. [b] Pseudorotation phase angle and conformational descriptor according to refs 58, 64, and 65. The pucker amplitudes ψ_m are between 41° and 47°. [c] Exocyclic torsion about C2′−C3′, $\theta \equiv \angle$(O2′, C2′, C3′, O3′). [d] Torsion about C1′−N9, $\chi \equiv \angle$(O4′, C1′, N9, C4). [e] Torsion about Sδ−Cγ, $\phi \equiv \angle$(C5′, Sδ, Cγ, Cβ). [f] From PDB 1RQP.

69° in SAM(B), and 75° in SAM(C), but 90° in **4.2** (as well as in the other optimized conformers). This rotates the S-methyl group toward the adenyl. (iv) Sulfonium pyramidalization: The sulfonium center is much less pyramidalized in SAM(A) than in all the calculated conformers. The improper torsion Sδ−C5′−Cγ−Cϵ is only 29° in SAM(A), but around 44° otherwise. For SAM(B) and SAM(C), it is 41° and 40°, respectively.

To gauge the energetic cost of these conformational features, we enforced them by successively constraining pertinent structural parameters to their value in SAM(A) and optimizing. The results are presented in Table 5. As reference, the data for **4.4**, resulting from free optimization of SAM(A), and SAM(A) itself are also included. Although fixing the Cϵ−C8 distance (**4.4g**) increases the energy only moderately, it leads to an entirely different ring conformation and does not appear to be relevant. Attempts to achieve the short Cϵ−C8 distance by torsion constraints only (**4.4a**−**e**), but preserving the essential conformational features of **4.4**, fail by almost 1 Å and cost 41 kJ mol^{-1}. Additionally imposing the distance constraint yields a conformation (**4.4f**) that is 74 kJ mol^{-1} above the freely optimized structure. By contrast, adjusting the ring conformation via one endocyclic torsion and rotating the C1′ and C4′ substituents about the connecting bonds (**4.4a**−**c**) does not significantly raise the energy with respect to **4.4**.

We believe that the exceptionally short Cϵ−C8 distance is likely to be an artifact of the X-ray diffraction refinement process, considering that (i) the conformation of SAM(A) is high in energy; (ii) there is in the enzyme no neighboring group that could exert steric strain on the sulfonium methyl group to push it toward C8; and (iii) the temperature factor is significantly higher for Cϵ than for the other SAM atoms. A possible reason could be an unoptimized or imbalanced set of force-field

Table 5. Constrained Conformations of SAM[a]

	ΔE/(kJ mol^{-1})[b]	constraints	P[c]	ψ_m[c]	θ[d]	χ[e]	χ'[f]	η[g]	ϕ[h]	d/Å[i]
4.4	0	none	100° ($^OT_1$)	43°	−18°	−98°	144°	91°	83°	4.80
4.4a	1	ν_2	87° ($^OT_4$)	43°	−7°	−99°	142°	91°	83°	4.86
4.4b	3	ν_2, χ'	87° ($^OT_4$)	43°	−7°	−120°	*120°*	90°	83°	4.75
4.4c	6	ν_2, χ', η	87° ($^OT_4$)	45°	7°	−121°	*120°*	*63°*	75°	4.37
4.4d	34	ν_2, χ', η, χ	87° ($^OT_4$)	50°	−9°	*−132°*	*120°*	*63°*	169°	4.25
4.4e	41	ν_{0-4}, χ', η, χ	*87°* ($^OT_4$)	*43°*	−11°	*−132°*	*120°*	*63°*	169°	3.99
4.4f	74	ν_{0-4}, χ', η, χ, π[j], d	*87°* ($^OT_4$)	*43°*	−10°	*−132°*	*120°*	*63°*	69°	*3.06*
4.4g	24	d	158° ($^2T_1$)	25°	−34°	−92°	151°	87°	66°	*3.06*
SAM(A)[k]			87° ($^OT_4$)	43°	−3°	−132°	120°	63°	149°	3.06

[a] Values in italic type are constrained. [b] Electronic energy relative to **4.4**. [c] Pseudorotation phase angle (P), conformational descriptor, and pucker amplitude (ψ_m) according to refs 58, 64, and 65. [d] Exocyclic torsion about C2′−C3′, $\theta \equiv \angle$(O2′, C2′, C3′, O3′). [e] Torsion about C1′−N9, $\chi \equiv \angle$(O4′, C1′, N9, C4). [f] Torsion about C1′−N9, $\chi' \equiv \angle$(C2′, C1′, N9, C4). [g] Torsion about C5′−Sδ, $\eta \equiv \angle$(C4′, C5′, Sδ, Cϵ). [h] Torsion about Sδ−Cγ, $\phi \equiv \angle$(C5′, Sδ, Cγ, Cβ). [i] Nonbonded distance Cϵ−C8. [j] Pyramidalization at C4′; π is the angle between the plane {O4′, C4′, C3′} and the vector {C4′, C5′}. [k] From PDB 1RQP.

Scheme 2. Reactivity Patterns of SAM[a]

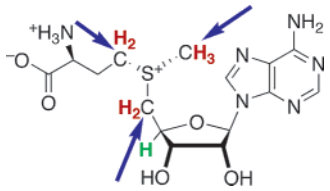

[a] Acidic α-protons (red); acidic β-proton (green); S_N2 attack (blue arrows).

parameters for SAM. We therefore do not expect to reproduce the experimental structure of SAM in these respects in the following QM/MM studies.

2. Reactivity of SAM Toward Fluoride. (a) Reactivity Patterns for SAM. As a second preparatory step for the QM/MM studies, the intrinsic reactivity of SAM toward fluoride was investigated. The fluoride ion is considered both as a base and as a nucleophile. Scheme 2 summarizes the possible reactivity patterns. (1) Acting as a base, fluoride can potentially abstract one of the acidic protons α to the sulfonium center, to generate a sulfur ylide. (2) Alternatively, deprotonation β to the sulfonium center at C4′ would lead to elimination of L-methionine and afford 4′,5′-anhydroadenosine. The resultant enol ether may be susceptible to HF addition and thus provide a path to 5′-FDA. (3) Considering fluoride as a nucleophile, it could attack at any of the three α-positions to form an alkyl fluoride and a thioether. Accordingly, we have studied the energetics of these different pathways to be able to assess the inherent propensity of SAM and fluoride for each alternative. As a fluoride ion in the gas phase is a poor model for solvated fluoride (especially with respect to basicity and nucleophilicity), all calculations reported here were performed in water as the continuum solvent.

(b) Fluoride as Base. Fluoride-mediated deprotonation at one of the three carbon atoms α to the sulfonium center yields the sulfur ylides **5a**−**c** and HF (Scheme 3). The corresponding reaction energies are collected in Table 6 (see the Supporting Information for gas-phase reaction energies and hydration energies). They are strongly endothermic, mostly owing to the loss of solvation energy upon combining two charged reactants into neutral products. We therefore do not consider mechanisms involving ylides any further in the present study.

Alternatively, fluoride can abstract the β-proton at C4′. The resulting anion is not stable but spontaneously eliminates L-methionine to form 4′,5′-anhydroadenosine (**6**), as shown in Scheme 4. This process is essentially thermoneutral (Table 6). Thus **6** emerges as a potential intermediate in the fluorination

Scheme 3. α-Deprotonation of SAM [**4.3**(aq)] Yielding the Sulfur Ylides **5a**−**c**

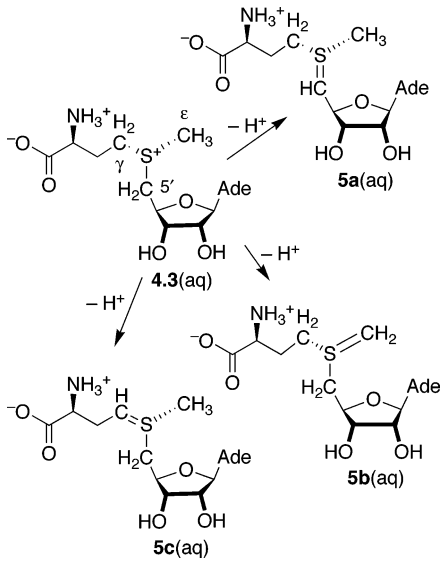

Table 6. Deprotonation and Substitution Reactions of SAM with F^-[a]

products	$\Delta_r E$/(kJ mol^{-1})
5a(aq) + HF(aq)	130
5b(aq) + HF(aq)	172
5c(aq) + HF(aq)	176
6(aq) + Met(aq) + HF(aq)	1
8(aq) + Met(aq)	−65
9(aq) + Met(aq)	−7
10(aq) + CH_3F(aq)	−3
11(aq) + **12**(aq)	−21

[a] Reaction energies for **4.3**(aq) + F^-(aq) → products.

reaction. The enol ether double bond in **6** is activated toward electrophilic attack. However, the textbook mechanism for electrophilic HX addition across an enol ether double bond gives the wrong regioisomer to that observed in the fluorination reaction. Protonation of **6** at the terminal end of the double bond affords the tertiary cation **7**, whose positive charge is supported by resonance stabilization with the adjacent ring oxygen. Assuming HF as the proton source, the corresponding reaction energy is 38 kJ mol^{-1}. **7** is then quenched by F^- to form (4′*S*)-4′-fluoro-5′-deoxyadenosine (**8**). This reaction is exothermic by −104 kJ mol^{-1} despite the substantial loss of solvation energy. The net reaction energy for this Markovnikov addition of HF to **6** is hence −66 kJ mol^{-1}.

However, the product of enzymatic fluorination is 5′-fluoro-5′-deoxyadenosine (5′-FDA, **9**), which is formally the result of

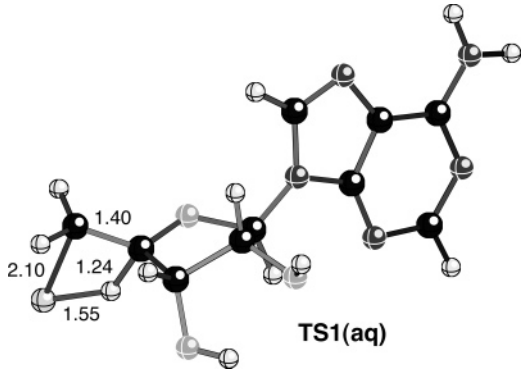

Figure 7. Transition state **TS1**(aq) for concerted anti-Markovnikov addition of HF(aq) to the enol ether **6**(aq). Selected distances are given in Å.

Scheme 4. β-Deprotonation of SAM [**4.3**(aq)] and Subsequent Elimination−Addition Reactivity

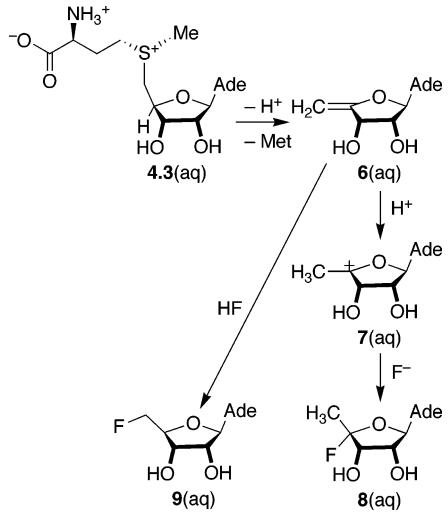

an anti-Markovnikov addition of HF to **6**. This process, **6**(aq) + HF(aq) → **9**(aq), has a net reaction energy of −8 kJ mol^{-1} and is thus also thermodynamically viable. But the intermediate primary cation, formed by protonation of the double bond of **6** at the 4′-position, is not stable. Depending on the details of the optimization, it readily undergoes a rearrangement (1,2-hydride shift, ring cleavage) to better stabilize the positive charge. Hence, we investigated the possibility of a concerted anti-Markovnikov addition of HF to **6**, which circumvents the unstable primary carbocation. We were indeed able to find a transition state for concerted HF addition (**TS1**), both in the gas phase (see Supporting Information) and in solution (Figure 7). The corresponding activation energy in solution is $\Delta^{\ddagger}E = 190$ kJ mol^{-1}.

The formation of 5′-FDA (**9**) from SAM via β-elimination of L-methionine, followed by concerted anti-Markovnikov addition of HF to enol ether **6**, is thus thermodynamically feasible, but prohibitive due to the high kinetic barrier for the addition step. We therefore exclude this pathway also for the enzymatic reaction, even if the initial elimination step might profit from generalized acid/base catalysis in the enzyme.

(c) Fluoride as Nucleophile. In view of the propensity of the sulfonium group to act as a leaving group, nucleophilic attack of F$^-$ at all of the three sulfonium α-carbon atoms of SAM was considered (Scheme 5). Attack at C5′ yields 5′-FDA (**9**) and L-methionine, the products obtained from the enzymatic reaction. Attack at Cϵ affords fluoromethane and *S*-adenosylhomocysteine (SAHC, **10**), which corresponds to the methyl

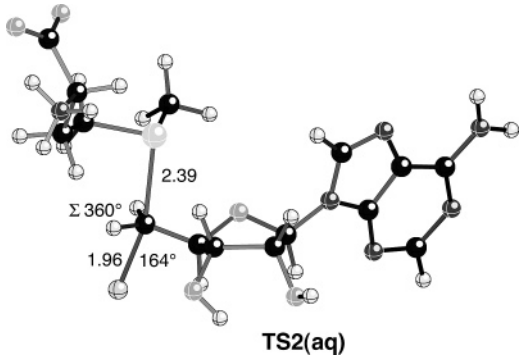

Figure 8. Transition state **TS2**(aq) for nucleophilic attack of F$^-$ at C5′ of SAM. Selected distances (Å) and angles (degree) are given.

Scheme 5. Nucleophilic Attack by Fluoride on SAM

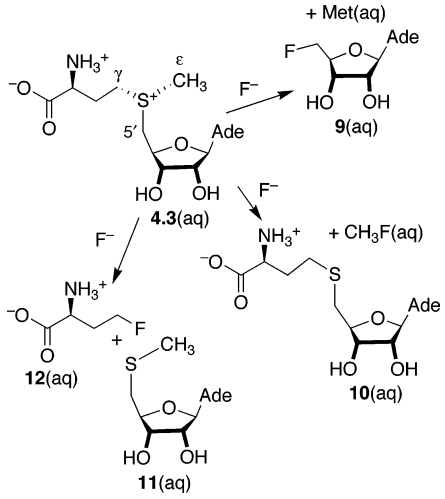

transfer reactivity often associated with SAM-dependent processes. Finally, attack at Cγ produces 5′-(*S*-methylsulfanyl)-5′-deoxyadenosine (**11**) and (*S*)-2-ammonio-4-fluorobutanoate (**12**). The energies for these reactions in solution are reported in Table 6 (see the Supporting Information for the corresponding gas-phase values and hydration energies). It emerges that all three substitution pathways are thermodynamically accessible, being slightly to moderately exothermic. There is no clear intrinsic energetic preference for either of them.

To be able to draw a comparison with the enzymatic reaction, we located the transition state for nucleophilic attack of fluoride to C5′ of SAM in solution, **TS2**(aq) (Figure 8). Its structure is characteristic for an S_N2 transition state. The C5′−F bond is partially formed [1.96 Å in the TS versus 1.42 Å in the product **9**(aq)], the C5′−Sδ bond is being cleaved [2.39 Å in the TS versus 1.86 Å in the reactant **4.3**(aq)], and the central carbon atom is absolutely planar. The attack is not perfectly linear, however, the angle F$^-$−C5′−Sδ being 164°. The activation energy for this process is $\Delta^{\ddagger}E = 92$ kJ mol^{-1} as calculated with the BP86 exchange-correlation functional. We performed single-point energy calculations for this reaction using the B3LYP functional. The barrier rises to 112 kJ mol^{-1}, while the reaction energy remains almost unaffected at −8 kJ mol^{-1}.

Summarizing the QM reactivity studies, we conclude that the formation of **9** via nucleophilic attack as observed in the enzyme concurs with the intrinsic reactivity of SAM and fluoride. This pathway is thermodynamically favored and kinetically feasible. The alternative elimination−addition mechanism that also leads

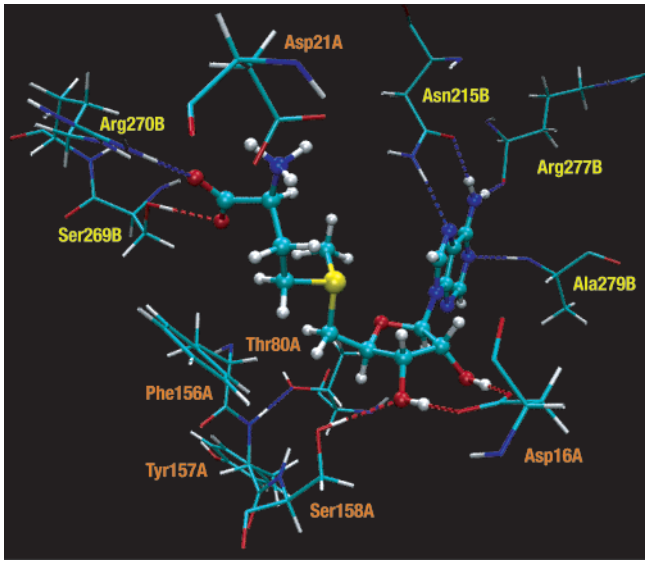

Figure 9. QM/MM-optimized structure of the SAM−enzyme complex. Selected residues around SAM are shown.

Table 7. Structural Parameters of SAM in QM/MM-Optimized Structures; Calculated Solution and Experimental X-ray Diffraction Data Are Included for Comparison

	P^a	$\psi_m{}^a$	θ^b	χ^c	η^d	ϕ^e	d^f/Å
4.3(aq)	80° ($^OT_4$)	47°	15°	−105°	91°	100°	5.07
SAM(A)[g]	87° ($^OT_4$)	43°	−3°	−132°	63°	149°	3.06
SAM−enzyme complex	76° ($^OT_4$)	33°	7°	−107°	91°	160°	3.96
reactant complex	85° ($^OT_4$)	33°	2°	−109°	83°	147°	3.76
TS3	78° ($^OT_4$)	37°	7°	−106°	88°	148°	3.73
product complex	69° ($^OT_4$)	41°	15°	−106°	79°	137°	3.84
FDA(A) + Met(A)[h]	73° ($^OT_4$)	47°	13°	−115°	103°	145°	3.88

[a] Pseudorotation phase angle (P), conformational descriptor, and pucker amplitude (ψ_m) according to refs 58, 64, and 65. [b] Exocyclic torsion about C2′−C3′, $\theta \equiv \angle$(O2′, C2′, C3′, O3′). [c] Torsion about C1′−N9, $\chi \equiv \angle$(O4′, C1′, N9, C4). [d] Torsion about C5′−Sδ, $\eta \equiv \angle$(C4′, C5′, Sδ, Cϵ). [e] Torsion about Sδ−Cγ, $\phi \equiv \angle$(C5′, Sδ, Cγ, Cβ). [f] Nonbonded distance Cϵ−C8. [g] From PDB 1RQP. [h] From PDB 1RQR.

Table 8. Selected H-Bonds in QM/MM-Optimized Structures (in Å)

	SAM–enzyme complex	reactant complex	**TS3**	product complex
Ser158A:(O)H···SAM(A):O3′	1.89			
Ser158A:(O)H···F$^-$		1.79	1.85	
Ser158A:(N)H···F$^-$		1.82	1.92	1.99
Thr80A:(O)H···F$^-$		1.82	2.04	
Tyr157A:(N)H···Thr80A:O(H)	1.83	1.91	1.89	2.02

to the observed products is not kinetically viable. The issue of regioselectivity, that is, which of the three α-carbon atoms is preferentially attacked, will not be further investigated here. For free SAM, attack at the methyl Cϵ is most likely to be kinetically preferred for steric reasons. In the enzyme, however, the regioselectivity is controlled entirely by the conformation and relative position of the reactants in the binding site.

B. QM/MM Studies. 1. SAM−Enzyme and Reactant Complex. The optimized structure of the active site of the SAM−enzyme complex is shown in Figure 9. Structural parameters of SAM are collected in Table 7 with hydrogen-bond distances in Table 8. SAM is bound by a number of hydrogen bonds and electrostatic interactions. The adenine base accepts hydrogen bonds from the side-chain amide NH_2 of Asn 215B and the backbone NH of Ala 297B; the adenine C6 amino group is hydrogen-bonded to the side-chain amide carbonyl of Asn 215B and the backbone carbonyl of Arg 277B. The methionyl carboxylate group accepts a hydrogen bond from the side-chain OH of Ser 269B and is stabilized by a salt bridge to the guanidinium side chain of Arg 270B. The positive charge of the methionyl ammonium group is compensated for by Asp 21A. The ribose C2′- and C3′-hydroxy groups are both hydrogen-bonded to the carboxylate side chain of Asp 16A, which fixes their orientation such that no intramolecular hydrogen bond can form. It also holds them in the almost fully synperiplanar arrangement. Additionally, O3′ is stabilized by a hydrogen bond from the Ser 158A side-chain OH. Compared to the crystal structure, this side chain has rotated by approximately 90° about the Cα−Cβ bond during the molecular dynamics simulations. Ser 158A also lines the empty binding site for fluoride, together with Tyr 157A, Phe 156A, and Thr 80A. The integrity of this pocket is stabilized by a hydrogen bond from the backbone NH of Tyr 157A to the side-chain oxygen of Thr 80A. Compared to **4.3**(aq), the ribose ring adopts the same pseudorotation phase but is significantly less puckered in the enzyme.

To generate the reactant complex from the SAM−enzyme complex, we inserted F$^-$ manually into its binding pocket such that it was at equal distance to obvious potential H-bond donors (Ser 158A side-chain OH and backbone NH; Tyr 157A backbone NH). Already the first MM-optimized structure revealed adaptations in the H-bonding network in and around the binding site. The Ser 158A side-chain OH is now orientated toward the fluoride, breaking the H-bond to O3′. Partially compensating for this, the backbone NH of Tyr 77A moves closer to the ribose OH groups. During the course of the MD simulations, the side-chain OH of Thr 80A also turned toward the fluoride. F$^-$ is hence stabilized in the binding pocket by hydrogen bonds from the Ser 168A side-chain OH and backbone NH as well as from the Thr 80A side-chain OH. The QM/MM-optimized structure of the reactant complex is shown in Figure 10; structural parameters for SAM and H-bond distances are listed in Tables 7 and 8, respectively.

The structural differences between SAM optimized in solution [**4.3**(aq)] and SAM in the SAM−enzyme or the reactant complex are rather small. Drawing on the results from the conformational survey, we estimate the strain energy for enzyme-bound SAM to be of the order of 10 kJ mol^{-1}. The distance of fluoride to the attacked carbon, d(F$^-$, C5′), is 2.75 Å; the attack angle, $\angle$(F$^-$, C5′, Sδ), is 165°. The sum of angles around C5′, as a measure for the degree of pyramidalization, is 331°, practically unchanged from the value in the SAM−enzyme complex (333°). Likewise for d(C5′, Sδ), which is 1.86 and 1.87 Å in the SAM−enzyme and the reactant complex, respectively.

2. Nucleophilic Attack and Product Complex. Starting from the reactant complex, we located the transition state for nucleophilic attack of the fluoride ion on C5′, **TS3**; see Figure 11, Tables 7 and 8. Its structure is very similar to the corresponding transition state in solution, **TS2**(aq) (Figure 8). The length of the forming bond is d(F$^-$, C5′) = 1.95 Å (1.96 Å in **TS2**); d(C5′, Sδ) is 2.48 Å (2.39 Å), elongated by 0.6 Å compared to the reactant complex; and $\angle$(F$^-$, C5′, Sδ) = 163° (164°). The central carbon C5′ is completely planar. The three hydrogen bonds supporting fluoride in the reactant complex are still present, however, elongated. The barrier is significantly

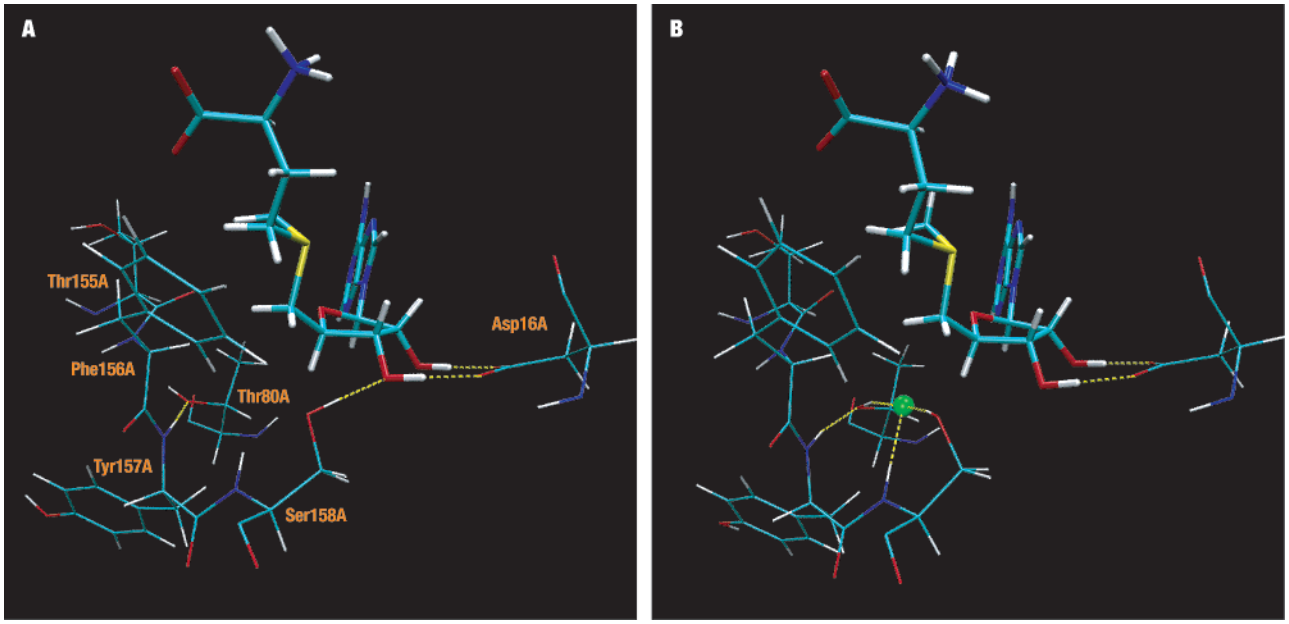

Figure 10. QM/MM-optimized structures of (A) the SAM−enzyme complex and (B) the reactant complex. Shown is SAM together with selected active-site residues.

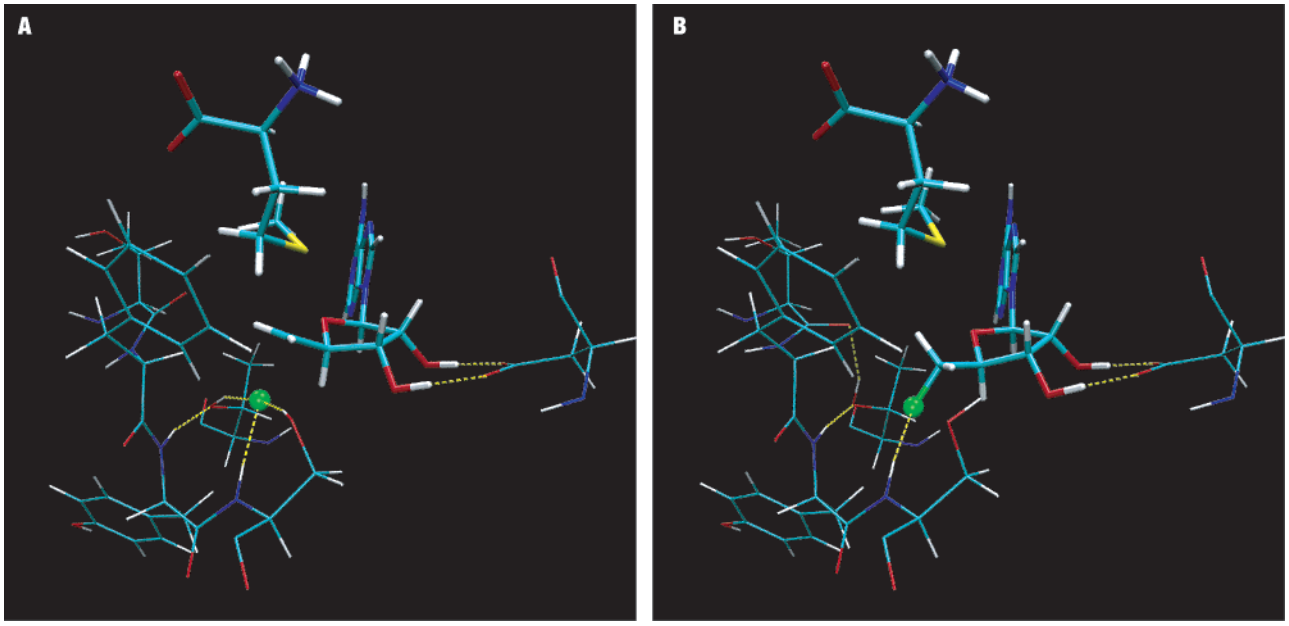

Figure 11. QM/MM-optimized structure of (A) the transition state **TS3** for nucleophilic attack and (B) the product complex. Identical view as that in Figure 10.

lowered compared to solution, $\Delta^{\ddagger}E = 53$ kJ mol^{-1}, versus 92 kJ mol^{-1} for **TS2**. Using B3LYP single-point energies, the corresponding values are 63 versus 112 kJ mol^{-1}.

Relaxing **TS3** toward the product side affords the product complex shown in Figure 11; see Tables 7 and 8 for structural information. The reaction energy in the enzyme is $\Delta_r E = -25$ kJ mol^{-1} relative to the reactant complex; the corresponding value in solution is -7 kJ mol^{-1} (Table 6). With B3LYP single-point energies, -34 and -8 kJ mol^{-1} are obtained, respectively. The products, 5′-FDA and L-methionine, have moved apart compared to **TS3**, d(C5′, Sδ) = 3.54 Å. The same hydrogen bonds contact the adenine part of 5′-FDA and the ammonio carboxylate of L-methionine, respectively. The H-bonding network around the fluorine, however, has rearranged, reflecting the change from the highly charged fluoride anion to the comparably nonpolar organofluoro substituent. Only the hydrogen bond from the Ser 158A backbone NH has remained. The Ser 158A side-chain OH has rotated away, and the Thr 80A side-chain OH now binds to the backbone carbonyl of Thr 155A. Compared to the X-ray structure of the product complex (PDB 1RQR), the fluoromethyl group is rotated. The torsion angle about C5′−C4′, $\kappa \equiv \angle$(F, C5′, C4′, O4′), is between 162° and 174° (+ap) for the three chains in the experimental structure, while it is 108° (+ac) in the QM/MM-optimized product complex. The fluorine thereby avoids close contact with the oxygen of the Ser 158A side-chain OH, which adopts in the QM/MM structure an orientation different from the crystal structure, as mentioned above.

To elucidate the factors that reduce the barrier in the enzyme by 39 kJ mol^{-1} compared to aqueous solution (49 kJ mol^{-1} if

B3LYP single-point energies are used), a decomposition scheme was applied that dissects the contributions related to changing the environment from solution to the enzyme. In the first stage, the changes upon transferring the reactants from solution into the enzyme are considered. This process can be subdivided into three steps, as shown in eq 1; "SAM" designates the part of SAM included in QM region, i.e., "SAM" = 5′-(*S*,*S*-dimethylsulfonio)-5′-deoxyadenosine.

$$\begin{aligned} &F^-(aq) + \text{“SAM”}(aq//aq) \\ &\xrightarrow[(i)]{\Delta_{prep}E(aq)} F^-(aq) + \text{“SAM”}(aq//enz) \\ &\xrightarrow[(ii)]{\Delta_{compl}E(aq)} [F^- \bullet \text{“SAM”}](aq//enz) \\ &\xrightarrow[(iii)]{\Delta_{QMMM}E} [F^- \bullet \text{“SAM”}](enz//enz) \end{aligned} \quad (1)$$

In step (i), the free, optimized reactants in water are distorted individually into the conformation that they have in the reactant complex in the binding site. Here, this concerns only "SAM", as fluoride has no internal structural degrees of freedom. "SAM"(aq//enz) thus corresponds to a single-point calculation on "SAM" in solution using its QM/MM-optimized structure. The (strictly positive) energy change associated with this preparation step is $\Delta_{prep}E(aq) = 40$ kJ mol^{-1}. It reflects the loss of the intramolecular hydrogen bond between the ribose OH groups as well as the conformational distortion. (ii) Next, the two reactants in water are brought into the relative position and orientation they adopt in the enzyme. The corresponding complexation energy (which can be either stabilizing or destabilizing) amounts to $\Delta_{compl}E(aq) = 22$ kJ mol^{-1}. This moderately positive value results from the loss of solvation energy overcompensating the attractive interaction between the two oppositely charged entities. In step (iii), the reactant complex is placed into the active site. The corresponding energy change $\Delta_{QMMM}E$ contains the difference in the electronic energy upon taking the QM charge density from solution into the field of the MM point charges, $\Delta_{QMMM}E_{QM}$, as well as the van der Waals interactions between QM and MM atoms, $\Delta_{QMMM}E_{vdW}$. Within the electrostatic embedding scheme employed here, $\Delta_{QMMM}E_{QM}$ includes the reorganization energy of the QM charge density as well as the electrostatic interaction between the density and the point charges. For the reactant complex,

$$\Delta_{QMMM}E = \Delta_{QMMM}E_{QM} + \Delta_{QMMM}E_{vdW} \quad (2)$$

both contributions to $\Delta_{QMMM}E$ are strongly stabilizing: $\Delta_{QMMM}E_{QM} = -535$ kJ mol^{-1}, $\Delta_{QMMM}E_{vdW} = -162$ kJ mol^{-1}.

In the second stage, we apply the analogous analysis to the TS itself, which enables a decomposition of the activation energy. Of particular interest is the barrier calculated in solution at enzyme-optimized structures, $\Delta^{\ddagger}E$(aq//enz), that is, for the process

$$[F^- \bullet \text{“SAM”}](aq//enz) \xrightarrow{\Delta^{\ddagger}E(aq//enz)} TS(aq//enz) \quad (3)$$

We obtain $\Delta^{\ddagger}E$(aq//enz) = 58 kJ mol^{-1}, which is only 5 kJ mol^{-1} higher than the full QM/MM barrier. Hence, the main role of the enzyme is to prepare the reactants and place them in a position suitable for reaction [steps (i) and (ii) above]. Its specific influence on the actual reactive event, however, is minor.

The full QM/MM barrier,

$$\Delta^{\ddagger}E(QM/MM) = \Delta^{\ddagger}E_{QM} + \Delta^{\ddagger}E_{MM} + \Delta^{\ddagger}E^{vdW}_{QMMM} \quad (4)$$

can be further dissected (neglecting link-atom corrections) into the contribution from the QM part, including the QM/MM electrostatic interaction, $\Delta^{\ddagger}E_{QM}$; the pure MM contribution (bonded, electrostatic, and van der Waals interactions between MM atoms), $\Delta^{\ddagger}E_{MM}$; and the contribution from the van der Waals interaction between QM and MM atoms, $\Delta^{\ddagger}E^{vdW}_{QMMM}$. $\Delta^{\ddagger}E_{QM}$, which corresponds to the sum of the intrinsic electronic barrier in the enzyme and the differential (de)stabilization of the TS by the MM point charges, amounts to 104 kJ mol^{-1} and is thus considerably higher than the full QM/MM barrier. The other two contributions are both stabilizing ($\Delta^{\ddagger}E_{MM} = -37$ kJ mol^{-1}, $\Delta^{\ddagger}E^{vdW}_{QMMM} = -14$ kJ mol^{-1}), reducing $\Delta^{\ddagger}E$(QM/MM) to the final value of 53 kJ mol^{-1} at the BP86 level.

Finally, the effect of the environment on the electronic structure of the reactants was investigated. The orbital interaction relevant for the nucleophilic attack is between the filled p-orbital of F^- pointing in the direction of C5′ and the empty C5′−Sδ antibonding orbital, σ^*_{C-S}. For the free reactants in solution, the energy gap between these two orbitals is 5.1 eV. Distorting the reactants into the conformation in the enzyme (step i) lowers σ^*_{C-S}, reducing the gap to 4.9 eV. Bringing the reactants into their final relative position (step ii) destabilizes both orbitals but leaves the gap unchanged. In the enzyme environment, that is, in the field of the point charges (step iii), the gap is reduced to 4.7 eV. This latter decrease by 0.2 eV thus reflects the specific action of the enzyme of promoting the reaction by creating a favorable electric field in the active site.

IV. Conclusions

The fluorinase is rare and unusual in biochemistry in that it is the only characterized native enzyme promoting the formation of C−F bonds. It catalyzes the reaction between *S*-adenosyl-L-methionine (SAM) and fluoride to form 5′-fluoro-5′-deoxyadenosine (5′-FDA) and L-methionine. We have used QM and QM/MM calculations to elucidate the mechanism of the C−F bond-forming step and obtain an insight into the role of the enzyme.

From the conformational survey that started from tetrahydrofuran (THF) and successively assembled SAM via 2,3-dihydroxy-THF and 1′-adenyl-2′,3′-dihydroxy-THF, we have found that the energetics of the conformational changes is dominated by hydrogen bonding, whereas the conformation of the ribose ring and relative orientations of substituents are less important. We estimate the conformational strain for enzyme-bound SAM to be of the order of 10 kJ mol^{-1}. The close contact between Cϵ and C8 observed in the X-ray structure is most likely artificial as it corresponds to a high-energy conformation for which no driving force exists.

We have also explored the intrinsic reactivity of SAM and fluoride in solution. Considering the possibility that fluoride will act as a base to abstract any of the acidic protons α to the sulfonium center, we find that the formation of sulfur ylides is highly endothermic and, hence, unlikely to be involved in, or compete with, the enzymatic reaction. On the other hand, an

elimination−addition pathway is in principle energetically viable. Removal of the hydrogen at C4′ of SAM triggers the elimination of L-methionine and the formation of an enol ether, to which HF can add concertedly in an anti-Markovnikov manner to yield 5′-FDA. The elimination is a favorable process energetically; however, the high barrier for the addition step (190 kJ mol^{-1}) excludes this pathway.

Nucleophilic attack of fluoride at any of the sulfonium α-carbon atoms is energetically favorable, without a clear thermodynamic preference for any of the three positions. The barrier in solution for attack at C5′, which yields the products observed in the enzymatic reaction, is 92 kJ mol^{-1} (112 kJ mol^{-1} at B3LYP//BP86). The reactivity patterns of SAM and fluoride in the enzyme and in solution therefore concur, and the enzyme acts only to modify the intrinsic reactivity.

The QM/MM calculations on the full enzymatic system were based on the experimental structure of the SAM−enzyme complex. Insertion of fluoride into the active site gave the reactant complex. The hydrogen-bonding network around the binding pocket rearranges to stabilize fluoride by hydrogen bonds from the side-chain OH and backbone NH of Ser 168A and from the side-chain OH of Thr 80A. The involvement of Thr 80A is not obvious from the X-ray structures. The fluoride ion is positioned at a distance of 2.75 Å from the electrophilic carbon C5′, with an F^{-}−C5′−Sδ angle of 165°. The barrier for nucleophilic attack in the enzyme is 53 kJ mol^{-1}, with an overall reaction energy of −25 kJ mol^{-1}. Using single-point B3LYP energies, the barrier is 63 kJ mol^{-1}, and the reaction energy is −34 kJ mol^{-1}. These results provide strong evidence that the C−F bond-forming step in the fluorinase follows an S_N2-type mechanism, corroborating experimental findings.

Assessing the complete enzymatic reaction cycle, the principal achievement of the fluorinase is certainly to bind, transport, and almost completely desolvate fluoride against its very high hydration free energy. With regard to C−F bond formation, the enzyme lowers the barrier by 39 kJ mol^{-1} compared to the reaction in aqueous solution (49 kJ mol^{-1} if B3LYP single-point energies are used), and this corresponds to a rate acceleration of more than 6 (8) orders of magnitude at room temperature. The major part of this barrier reduction is related to structural rearrangements, preparing and placing the reactants in a position suitable for reaction. The specific barrier lowering due to the protein environment at optimized QM/MM geometries is computed to be only 5 kJ mol^{-1} compared to aqueous solution. The promoting influence of the enzyme environment on the electronic structure of the reactants is reflected in a reduced energy gap between the relevant frontier orbitals owing to both structural distortion and the electric field in the active site.

Acknowledgment. We are grateful to Prof. J.H. Naismith (University of St. Andrews) for making the coordinates of 1RQP and 1RQR available to us before publication. We thank Prof. A. MacKerell (University of Maryland), Prof. B. Roux (Cornell University), and Prof. P. Jordan and Dr. G. Miloshevsky (Brandeis University) for providing us with CHARMM force field parameters. Dipl.-Biochem. N. Otte (MPI für Kohlenforschung) is acknowledged for help with the CHARMM setup. Dr. B. Ganguly (CSIR Laboratory, Bhavnagar, India) is thanked for contributing to the CHARMM parameter development and the QM reactivity studies.

Supporting Information Available: Details on QM calculations, system preparation, the MM parameter development, and QM/MM setup; QM gas-phase results; and complete citations for refs 51 and 57 (PDF). Coordinates of all optimized structures (multipart Xmol xyz format); QM/MM-optimized structures in PDB format. This material is available free of charge via the Internet at http://pubs.acs.org.

JA053875S